Journal of Catalysis **184,** 189–201 (1999)
Article ID jcat.1999.2417, available online at http://www.idealibrary.com on IDEAL®

Dynamic Behavior of Adsorbed NO and CO under Transient Conditions on Pd/Al_2O_3

Khalid Almusaiteer and Steven S. C. Chuang[1]

Department of Chemical Engineering, The University of Akron, Akron, Ohio 44325-3906

Received October 22, 1998; revised January 4, 1999; accepted January 5, 1999

The dynamic behavior of adsorbed NO and CO under transient NO–CO reaction conditions on Pd/Al_2O_3 has been studied by *in situ* infrared (IR) spectroscopy coupled with TPR and pulse reaction techniques in the 303–673 K range. Below the light-off temperature (i.e., 561 K), Pd^0–NO and Pd^0–CO are the dominant adsorbates on the Pd surface. Pd^0–NO competes favorably over Pd^0–CO for the same reduced Pd^0 site when the temperature is increased. Pulse reaction studies at 473 K suggest that Pd^0–NO dissociates to form adsorbed nitrogen and adsorbed oxygen. Adsorbed oxygen further reacts with Pd^0–CO to produce CO_2. Concentration profiles of CO_2 and Pd^0–CO during the pulse reaction studies indicate that removal of adsorbed oxygen from the Pd surface to produce CO_2 is the rate-limiting step. Prolonged exposure of the catalyst to the NO flow at 473 K results in oxidation of Pd^0 to Pd^+ and produces Pd–NO^+; the presence of gaseous CO reduces Pd^+ to Pd^0 and increases the surface coverage of Pd^0–NO. Above the light-off temperature, Pd–NO^+, Al–NCO, nitrate, and carbonate species are the dominant adsorbates. The presence of Pd–NO^+ indicates that the process for Pd^0 oxidation to Pd^+ by NO is faster than that of Pd^+ reduction to Pd^0 by CO. This study demonstrates that careful selection of transient IR techniques allows (i) determination of the modes of adsorbed NO and CO participating in the reaction and (ii) development of a comprehensive mechanism for the NO–CO reaction on Pd/Al_2O_3 catalyst.

Key Words: **Pd (palladium); Pd/Al_2O_3; infrared spectroscopy (IR); adsorbed NO; adsorbed CO; chemisorption; NO–CO reaction; NO reduction; pulse reaction; temperature-programmed reaction (TPR); mechanism; rate-limiting step; reaction dynamics; transient condition.**

INTRODUCTION

Carbon monoxide (CO) and nitric oxide (NO) are considered the major pollutants from automobile emissions. Removal of CO and NO from the automobile exhaust is an important subject in environmental catalysis (1–5). In a conventional catalytic converter, Rh and Pt are used for simultaneous control of CO, NO, and hydrocarbons (HC) emissions. Due to limited supply and elevated cost of Rh, automobile producers have introduced the palladium catalyst as a substitute for Rh and Pt (4). Successful development of Pd-based catalysts for the catalytic converter has been attributed to the excellent durability of Pd compared to that of Rh/Pt. While the total cost of Rh/Pt catalytic converter is close to that of Pd-only catalytic converter, Pd-only automotive catalysts provide an alternative to the monopolistic usage of Rh for automobile NO emission control. However, there are some drawbacks in using Pd, such as the susceptibility of Pd to poisoning by sulfur, phosphorus, lead, and zinc (4–6).

Continuing improvement of Pd catalyst to meet increasingly stringent requirements for NO emission control requires a comprehensive understanding of the NO–CO reaction mechanism on Pd. Understanding of Pd catalysis of the NO–CO reaction has been achieved by spectroscopic studies of NO and CO adsorption and steady-state and surface science studies of Pd single crystal and supported metal catalysts (7–11). Spectroscopic studies have shown that NO chemisorbs on a Pd surface as cationic NO [Pd–NO^+], linear NO [Pd^0–NO], and bent NO [Pd–NO^-]; CO chemisorbs as linear CO [Pd^0–CO] and bridged CO [$(Pd^0)_2$–CO] (7–12). Although these adsorbates on the Pd surface may serve as active precursors involved in surface reactions for N_2 and CO_2 formation, little attempt has been made to correlate the mode and concentration of adsorbates with the catalyst activity.

Investigation of the dynamic behavior and reactivity of various modes of adsorbed NO and CO by transient techniques could provide mechanistic information regarding active and spectator adsorbates as well as the change in behavior of the adsorbates and catalyst surface due to variation in reactant concentration (13, 14). In the present work, temperature programmed reaction (TPR) and pulse reactions were used to determine the nature of active sites and reactivity of various adsorbates under transient conditions as well as to verify and improve the general form of the proposed mechanism for the NO–CO reaction on Pd-based catalysts. Fourier transform infrared (FTIR) spectroscopy was used to monitor the transient responses of adsorbates,

[1] To whom correspondence should be addressed. E-mail: schuang@uakron.edu.

0021-9517/99 $30.00

and mass spectrometry (MS) was used to determine the response to the changes in concentration of gaseous products in the effluent of the IR reactor cell during TPR and pulse reaction studies.

EXPERIMENTAL

The Pd/Al_2O_3 catalyst was prepared by incipient wetness impregnation of γ-Al_2O_3 support (Alfa Chemicals, 100 m^2/g) with $PdCl_2$ (Alfa Chemicals) solution at a pH of 2.8 and 60°C (7). The catalyst was calcined by flowing air at 673 K for 8 h and then was reduced at 673 K in flowing H_2 for 8 h. The Pd loading was determined to be 1.75 wt% by inductively coupled plasma (ICP) emission spectroscopy (Galbraith Laboratories Inc.). The dispersion of Pd atoms, determined by the H_2 pulse chemisorption method at 303 K, was 16%, corresponding to the average Pd crystallite size of 60 Å. The X-ray diffraction (XRD) technique was used to further confirm the crystallite size and the Pd atoms dispersion. The average Pd crystallite size, determined by XRD, was 64 Å, corresponding to a 13% dispersion of Pd atoms.

The catalyst was pressed into a self-supporting disk and placed in the IR reactor cell for *in situ* transmission IR studies. Prior to the reaction studies, the catalyst was reduced *in situ* at 673 K for 2 h and no further reduction was done between the experiments to emulate the practical conditions existing in an automotive catalytic converter where the catalyst is not periodically reduced.

The experimental system, shown in Fig. 1A, consists of (i) a gas flow section with a six-port pulsing valve, (ii) an *in situ* IR reactor cell with a self-supporting catalyst disk section, and (iii) an analysis section with MS. At a total flow rate of 40 cm^3/min, it takes 10 s for a NO or CO pulse to travel from the pulse injection valve to the IR reactor cell and 24 s from the IR reactor cell to MS. Details of the IR reactor cell and piping have been presented elsewhere (14). Figure 1B

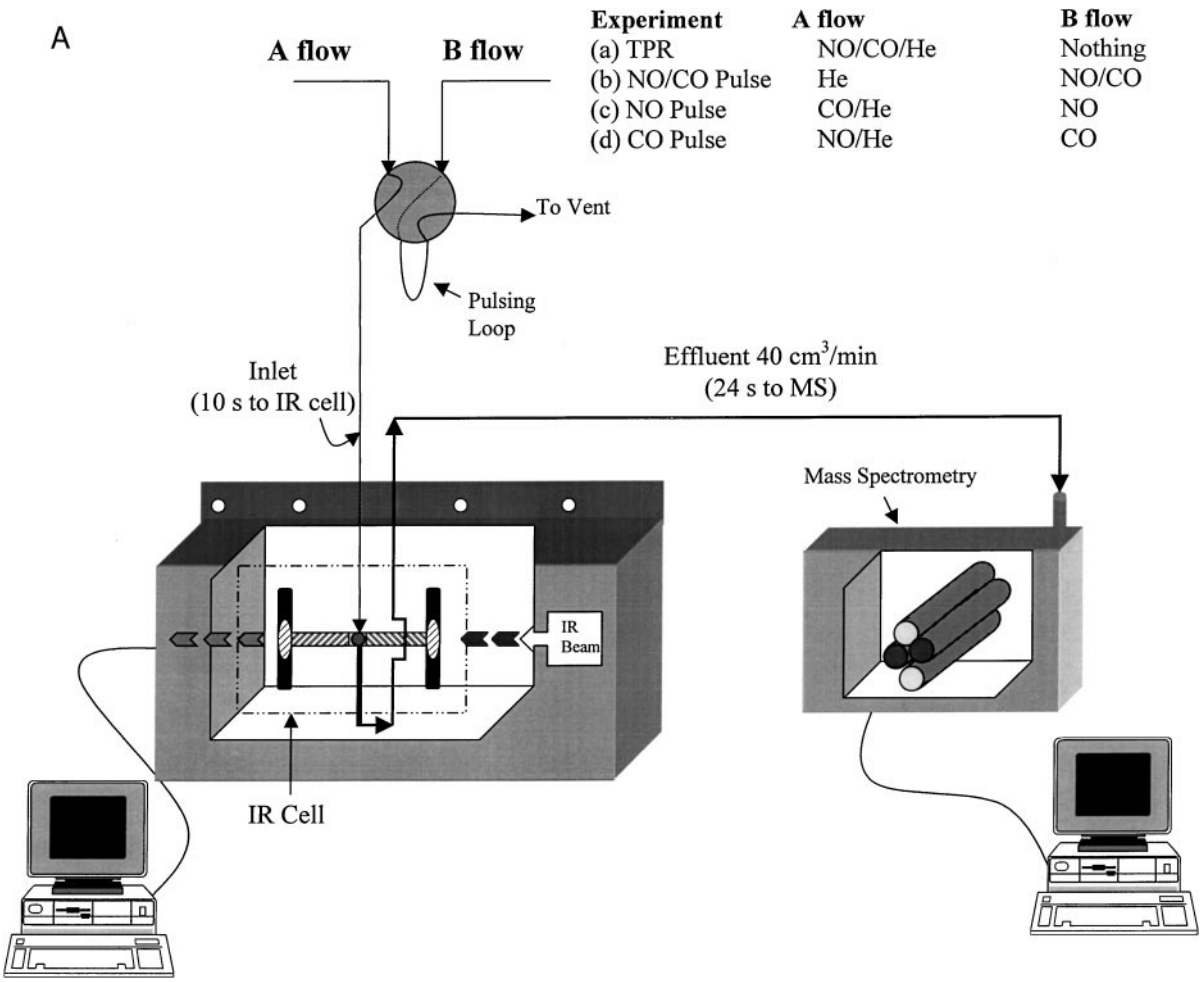

FIG. 1. (A) The experimental system consists of (i) a gas flow section with a six-port pulsing valve, (ii) an *in situ* IR reactor cell with a self-supporting catalyst disk section, and (iii) an analysis section with MS. (B) Experimental approaches: (a) Temperature programmed reaction (TPR) NO/CO/He (10/10/30 cm^3/min). (b) The NO/CO (5/5 cm^3) pulse into He (30 cm^3/min) flow. (c) The NO (10 cm^3) pulse into CO/He (10/30 cm^3/min) flow. (d) The CO (10 cm^3) pulse into NO/He (10/30 cm^3/min) flow.

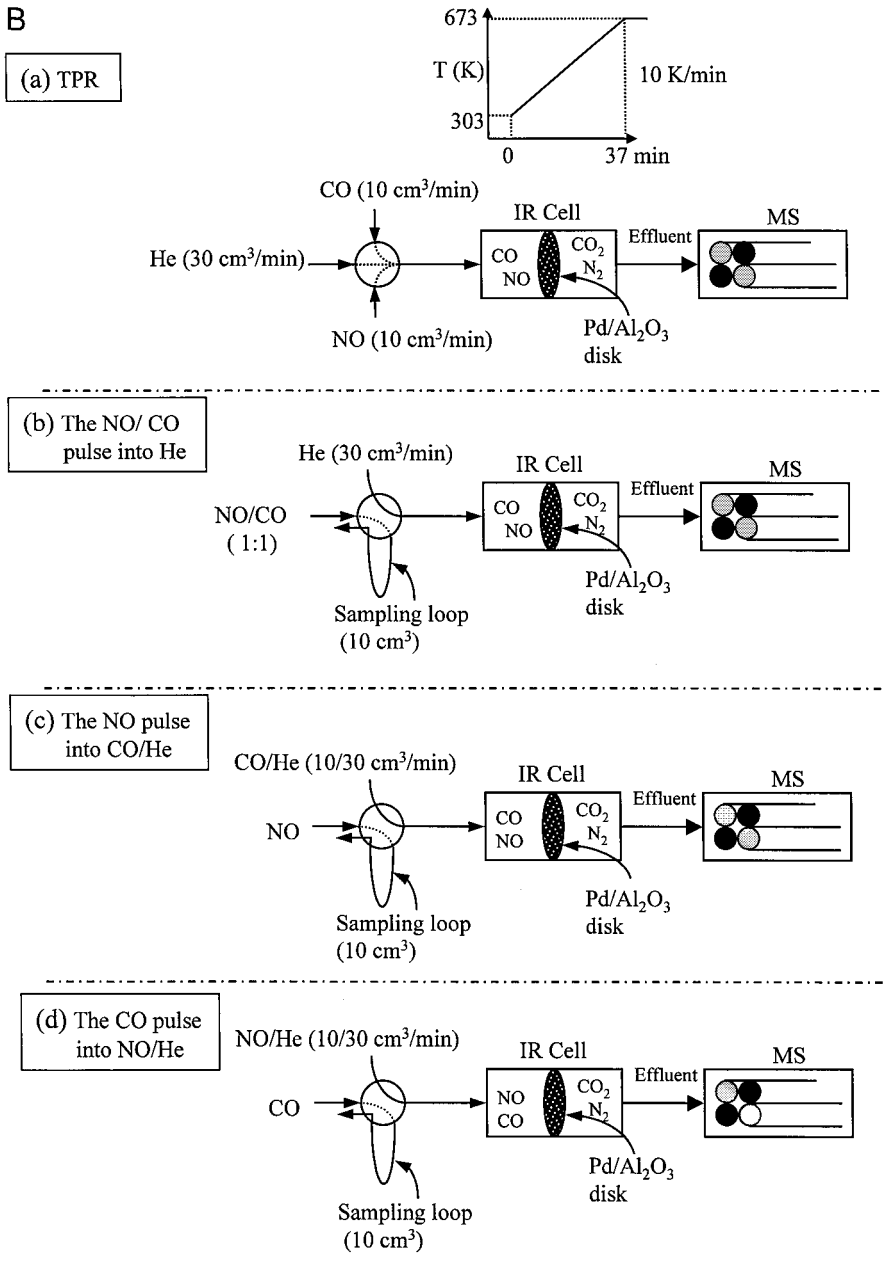

FIG. 1—*Continued*

(a–d) illustrate the experimental approaches used in this study, which consist of (a) IR–temperature programmed reaction (IR–TPR), (b) pulse injection of NO/CO mixture into a He flow, (c) pulse injection of NO into a CO/He flow, and (d) pulse injection of CO into a NO/He flow. Pulse injection experiments were carried out in the order (b), (c), and (d), shown in Fig. 1B.

The variation in concentration of adsorbates was monitored by FTIR and that of gaseous products and reactants was monitored by MS. The gaseous MS responses for m/e ratios corresponding to CO and N_2 ($m/e = 28$), NO ($m/e = 30$), as well as CO_2 and N_2O ($m/e = 44$) were monitored. The CO_2 and N_2O ($m/e = 44$) responses can be separated using the calibrated response ratio of the primary ionization fragment ($m/e = 44$) and the secondary ionization fragment ($m/e = 22$) of CO_2.

RESULTS

IR–TPR of NO/CO/He

Figures 2a and 2b show the IR spectra of adsorbates and the MS intensity of the effluent from the IR reactor cell during the NO/CO/He TPR as a function of temperature.

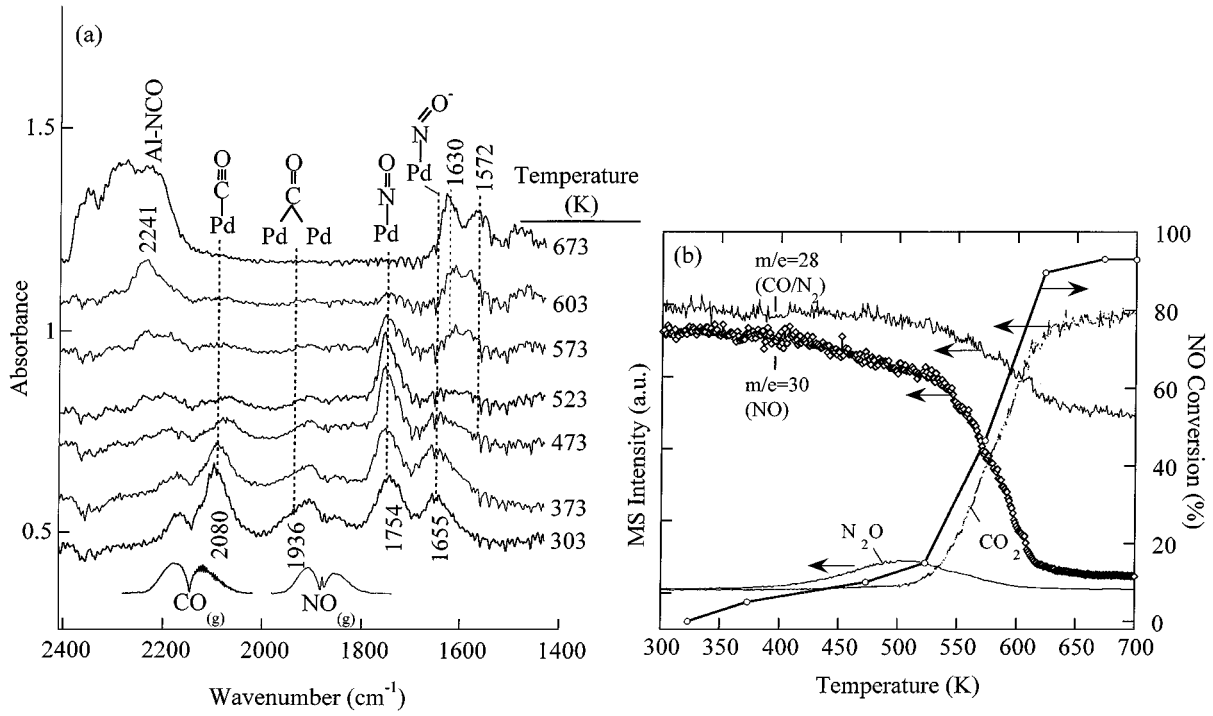

FIG. 2. (a) Transient IR spectra during the NO/CO/He (10/10/30 cm^3/min) TPR (10 K/min). (b) MS intensity profile of the effluent from the IR reactor cell.

Flowing the NO/CO/He reactant mixture over the catalyst at 303 K produced linear CO [Pd^0–CO] at 2080 cm^{-1}, bridged CO [$(Pd)_2$–CO] at 1950 cm^{-1}, linear NO [Pd^0–NO] at 1754 cm^{-1}, and bent NO [Pd–NO^-] at 1655 cm^{-1}. The $(Pd^0)_2$–CO band overlapped with the gaseous NO band, broadening the *P* branch of the gaseous NO band; the Pd^0–CO band overlapped with the gaseous CO band, intensifying the *R* branch of the gaseous CO band. The overlapping can be clearly discerned from comparison of IR spectra of adsorbates with gaseous NO and CO bands presented in Fig. 2a.

Figure 2b shows that the NO conversion took off at 520 K, where Pd^0–CO and Pd–NO^- depleted; and the Pd^0–NO increased to the maximum shown in Fig. 2a. Fifty percent conversion of NO was achieved at 561 K, which is termed the light-off temperature of the reaction. At the light-off, the major IR bands are Pd^0–NO, isocyanate on the support (Al–NCO) at 2241 cm^{-1} (11, 15–18), nitrate at 1630 cm^{-1}, and carbonate at 1572 cm^{-1} (19). Variation in adsorbate intensity between 303 and 561 K reflects changes in their surface coverage due to differences in dependence of adsorption, desorption, and surface reaction rates on temperature. Above the light-off, the NO conversion shoots up from 49% at 575 K to 94% at 673 K; Al–NCO and nitrate intensities increased with temperature, while Pd^0–NO depleted its intensity. The depletion of adsorbates on Pd (i.e., Pd^0–CO, $(Pd^0)_2$–CO, Pd^0–NO, and Pd–NO^-) suggests that the reaction falls into the region of the internal diffusion control in which little NO and CO penetrate into the catalyst pore for the adsorption and surface reaction (20). These depleted adsorbates may be active adsorbates toward product formation while those present on the catalyst surface may be spectators.

The infrared extinction coefficients of Pd^0–CO and Pd^0–NO were determined to be 0.61 and 0.79 cm/μmol, respectively, by pulse chemisorption at 303 K and 0.1 MPa. The similarity in the extinction coefficients allows direct use of Pd^0–CO and Pd^0–NO intensity as a measure of their relative surface coverages. Table 1 lists the TOF_{NO} (turnover frequency for NO conversion) measured at steady-state flow condition during TPR. It should be noted that TOF_{NO} at 573 and 623 K are not reliable due to the diffusion limitation and deviation from differential conditions.

NO/CO Pulse into He Flow

The objective of this study is to investigate the competitive adsorption of NO and CO as well as the sequence of adsorbate and product formation. Figure 3a shows the IR spectra of the adsorbates during the NO/CO pulse into He flow at 473 K. The pulse was made at time = 0 s. Thirty-three seconds were needed for the NO/CO to produce Pd^0–CO at 2065 cm^{-1} and Pd^0–NO at 1754 cm^{-1}. At 36 s, the Pd–NO^- band at 1649 cm^{-1} and nitrato at 1448 cm^{-1} as well as gaseous CO_2 and N_2O emerged.

As the NO/CO pulse traveled over the catalyst disk, the intensity of adsorbates, reactants, and products increased to

TABLE 1

Conversion (X) and Selectivity (S) during the Pulse Studies

Temperature (K)	TOF[a] (s^{-1})	Conversion and selectivity (%)								
		Pulse NO/CO			Pulse NO into CO			Pulse CO into NO		
		X_{NO}[b]	X_{CO}[c]	S_{N_2}[d]	X_{NO}	X_{CO}	S_{N_2}	X_{NO}[e]	X_{CO}	S_{N_2}
473	0.7	42 (5)[f]	34	33 (96)[g]	30 (5)	22	31 (55)	30	27	100
523	1.1	34 (7)	22	41 (84)	33 (4)	45	17 (82)	12	32	100
573	3.3	63 (42)	76	84 (99)	44 (18)	58	72 (80)	65	69	100
623	6.4	92	94	76	55	67	65	91	96	100

[a] From TPR results.

[b] $X_{NO}\,(\%) = \frac{\text{mol NO}_{in} - \text{mol NO}_{out}}{\text{mol NO}_{in}} \times 100\%$.

[c] $X_{CO}\,(\%) = \frac{\text{mol CO}_2}{\text{mol CO}_{in}} \times 100\%$.

[d] $S_{N_2}\,(\%) = \frac{\text{mol N}_2}{\text{mol N}_2 + \text{mol N}_2\text{O}} \times 100\%$.

[e] $X_{NO}\,(\%) = \frac{\text{mol N}_2}{\text{mol NO}_{in}} \times 100\%$.

[f] $X_{NO}\,(\%) = \frac{\text{NO (\%) on Rh/SiO}_2 \times \text{(No. active Pd sites)}}{\text{(No. active Rh sites)}}$.

[g] S_{N_2} on Rh/SiO_2.

a maximum and then decreased. Variation of the adsorbate IR intensity with time is plotted along with the MS intensity of the effluent from the IR reactor cell in Figs. 3b and 3c, respectively, to highlight the lead-lag relationship between reactants, adsorbates, and products. Since it takes 24 s for the gaseous species to travel from the IR reactor cell to the MS detector, the time of the MS results, for this and the subsequent figures was adjusted to represent that of gaseous species in the IR reactor cell. Gaseous NO, the reactant, lagged behind Pd^0–NO due to the delay caused by NO adsorption/desorption processes. The lead–lag relation between gaseous CO and adsorbed CO cannot be discerned because of the overlapping of N_2 and CO MS signals. The leading portion of $m/e = 28$ appears to be due to N_2 formed by the reaction. The frontal of the N_2 profile coincided with that of CO_2, indicating that the difference in dynamics of their formation are too small to be distinguished by the time-resolution of the MS used. The frontal profile for the formation of these products clearly lagged behind those of Pd^0–CO and Pd^0–NO. This observation is consistent with the general concept of catalysis where the reactants adsorb to form adsorbates for conversion to products. As a result, the product should lag behind the adsorbate.

After the NO/CO pulse left the IR reactor cell, gaseous NO and CO_2, as well as Pd^0–CO, show a rapid decay in their intensity (i.e., concentration) with time (Figs. 3b and 3c). In contrast, Pd^0–NO shows a slow decay in its IR intensity due to strong adsorption (Fig. 3b). The conversion and selectivity during the pulse studies reaction are listed in Table 1.

Since the behavior of adsorbates and the formation rate of products below light-off (e.g., 473 K) differ from those above light-off, it is worthwhile to investigate the reaction above light-off (e.g., at 623 K). Figures 4a–4c show the IR spectra of adsorbates, variation in the IR intensity of adsorbates, and the MS intensity of the effluent from the IR reactor cell during the NO/CO pulse at 623 K. Pulsing NO/CO produced the Pd–NO^+ band at 1803 cm^{-1} at 33 s; Al–NCO at 2243 cm^{-1}, as well as the nitrato and carbonate species in the 1500–1630 cm^{-1} range at 36 s. Adsorbed CO was not observed due to its high reactivity. The appearance of the Pd–NO^+ band indicates occurrence of oxidation of Pd^0 to Pd^+, which may be associated with adsorbed oxygen produced by NO dissociation. The disappearance of the Pd–NO^+ band at 54 s indicates the reduction of Pd^+ to Pd^0 by CO. Following the decrease in Pd–NO^+ is an immediate increase in the MS profile of N_2O and a significant increase in the IR intensity of Al–NCO.

Pulse NO into CO/He Flow

The NO–CO reaction is a redox reaction where NO serves as an oxidizing agent and CO a reducing agent. Flowing NO alone over the catalyst should oxidize a large portion of Pd^0 to Pd^+ while flowing CO could reverse the process. The objective of this study is to determine the effect of the surface state (e.g., Pd^0 and Pd^+) on the mode and reactivity of adsorbates. Figures 5a–5c show the IR spectra, variation in the IR intensity of adsorbates, and the MS intensity of the effluent from the IR reactor cell during the NO pulse into the steady-state CO/He flow at 473 K. Exposure

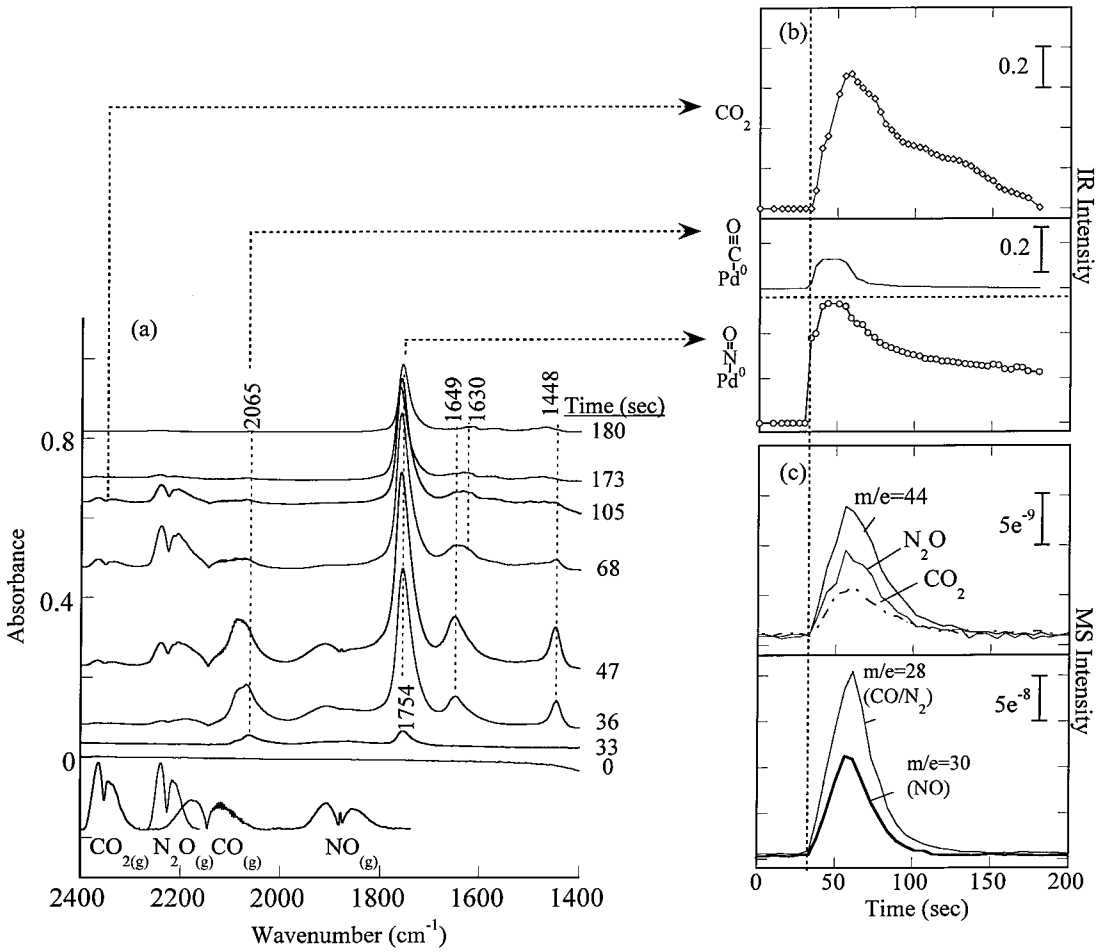

FIG. 3. (a) Transient IR spectra during the NO/CO pulse (5/5 cm^3) into He (30 cm^3/min) flow at 473 K. (b) Integrated area of IR intensity as a function of time. (c) MS intensity profile of the effluent from the IR reactor cell.

of the catalyst surface to CO/He flow resulted in the appearance of Pd^0–CO at 2065 cm^{-1}, $(Pd^0)_2$–CO at 1925 and 1869 cm^{-1}, and carbonate species in the 1400–1600 cm^{-1} range. The observation of Pd^0–CO and $(Pd^0)_2$–CO indicates that the Pd surface was in the Pd^0 state prior to the NO pulse. The steady-state flow of CO was needed for the formation of carbonate species which was absent during the NO/CO pulse at 473 K (Fig. 3a).

Pulsing NO into the CO/He flow produced Pd^0–NO (1754 cm^{-1}) at 28 s and Pd–NO^- (1650 cm^{-1}) at 33 s. The Pd–NO^- lagging behind Pd^0–NO had also been observed during the NO/CO pulse as shown in Fig. 3a. An increase in the intensity of Pd^0–NO and Pd–NO^- was accompanied by a decrease in that of Pd^0–CO and $(Pd^0)_2$–CO as well as an increase in the IR and MS intensity of CO_2 and N_2O. The CO_2 MS profile lagged behind that of N_2O in Fig. 5c, suggesting that the $NO_{ad} + N_{ad} \rightarrow N_2O$ reaction is faster than the $CO_{ad} + O_{ad} \rightarrow CO_2$ reaction.

As gaseous NO left the reactor, both Pd^0–NO and Pd–NO^- showed a rapid decrease in their intensity as compared to gaseous NO reactant as well as N_2O and CO_2 products. The majority of the adsorbates returned to their initial intensity except Pd^0–CO, which lost 15% of its initial intensity. The second NO pulse into the CO/He flow showed that the catalyst also lost 15% of its initial activity for NO reduction.

Figures 6a–6c show the IR spectra, variation in the IR intensity of adsorbates, and the MS intensity of the effluent from the IR reactor cell during the NO pulse into the CO/He flow at 623 K. Exposure of the catalyst to CO/He flow produced $(Pd)_2$–CO centered at 1945 cm^{-1} and carbonate species in the 1400–1640 cm^{-1} range. The Al–NCO band at 2245 cm^{-1} was formed by the NO pulse at low temperatures. Pulsing NO caused the following: (i) a decrease in the intensity of $(Pd^0)_2$–CO, Al–NCO, and carbonate species, (ii) an appearance of Pd^0–NO at 1752 cm^{-1}, Pd–NO^+ at 1798 cm^{-1}, and Pd–NO^- at 1677 cm^{-1} at 33 s, and (iii) an increase in CO_2 and N_2O formation.

Figures 6b and 6c highlight the lead–lag relationship of the variation in reactants, adsorbates, and products. The rising portion of Pd–NO^+ followed that of gaseous NO.

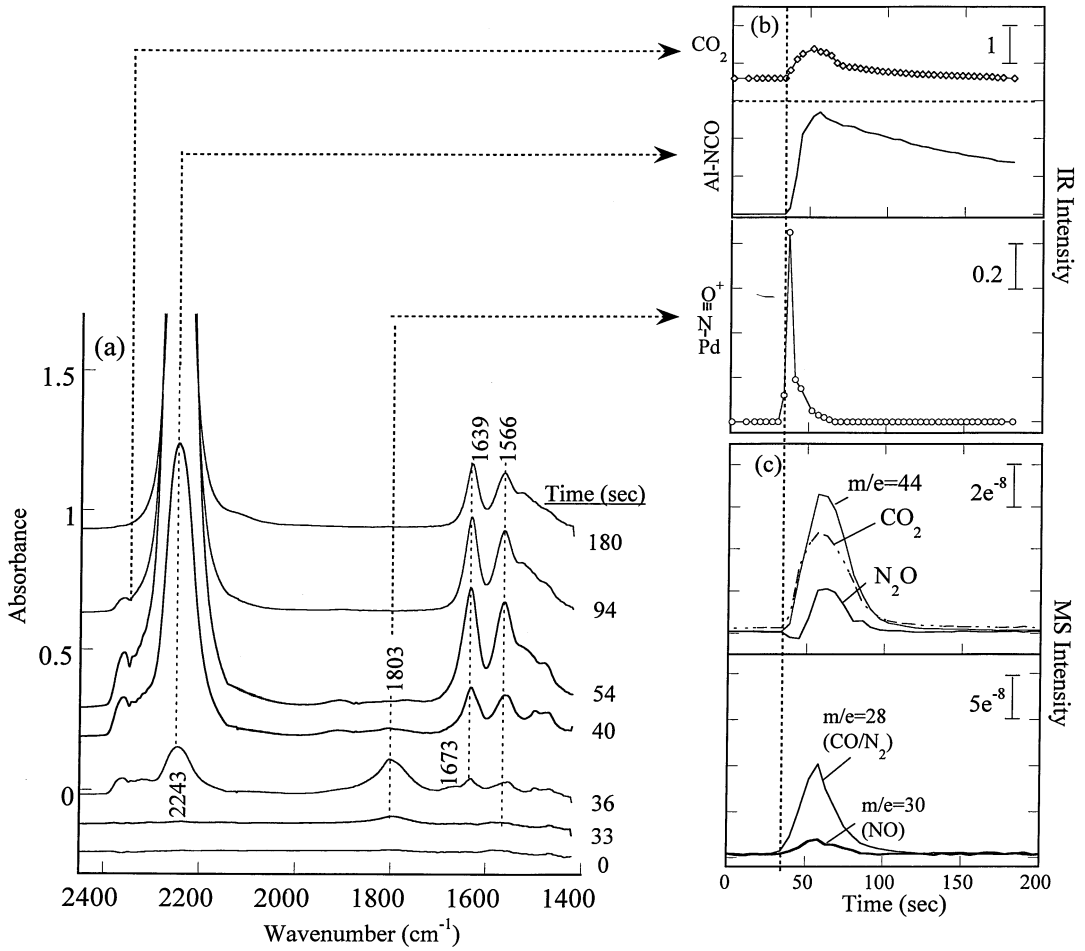

FIG. 4. (a) Transient IR spectra during the NO/CO pulse (5/5 cm^3) into He (30 cm^3/min) flow at 623 K. (b) Integrated area of IR intensity as a function of time. (c) MS intensity profile of the effluent from the IR reactor cell.

As Pd–NO^+ decreased in intensity, $(Pd^0)_2$–CO showed a gradual increase in its intensity while Al–NCO and N_2O showed a marked increase in their intensities, suggesting that the formation of N_2O and Al–NCO occurred after Pd^+ was reduced to Pd^0.

Pulse CO into NO/He Flow

Figures 7a–7d show the IR spectra, variation in the IR intensity of adsorbates, and the MS intensity of the effluent from the IR reactor cell during the CO pulse into the steady-state NO/He flow at 473 K. Prolonged exposure of the catalyst to NO flow resulted in the prevalence of adsorbed oxygen on the surface. Adsorbed oxygen could oxidize Pd^0 to Pd^+. The formation of Pd^+ is evidenced by the presence of Pd–NO^+ at 1779 cm^{-1}. Prolonged NO exposure also produced Pd–NO^- at 1677 cm^{-1} and the nitrate species in the 1472–1616 cm^{-1} range.

Pulsing CO into the NO/He flow produced CO_2 and Pd–NCO (2159 cm^{-1}) at 29 s; Pd–CO at 2083 cm^{-1} and $(Pd^0)_2$–CO centered at 1966 cm^{-1} appeared at 33 s. It should be noted that the intensity of Pd–CO increased with its wavenumber from 2065 cm^{-1} in Figs. 3a and 5a to 2083 cm^{-1} in Fig. 7a due partly to the dipole–dipole interaction and the presence of some Pd^+ sites. Since the high intensity of Pd–NO^+ species veiled the subtle changes in the intensity of other adsorbates, the variation in the IR intensity of CO and NO adsorbates on Pd is further highlighted by the difference spectra in Fig. 7b. A positive band indicates an increase in surface coverage and vice versa for a negative band. Close examination of the change in the intensity of IR-observable species reveals the following: (i) an initial increase followed by a rapid decrease in the intensity of the Pd–NO^+ at 1779 cm^{-1}, (ii) an increase in the intensity of Pd–NO^- accompanied by the downward shift in its wavenumber to 1652 cm^{-1}, and (iii) an appearance of Pd^0–NO at 1754 cm^{-1} at 58 s followed a maximum concentration of Pd–CO at 47 s. The appearance of Pd^0–NO indicates occurrence of reduction of Pd^+ into Pd^0. Simultaneous appearance of Pd^0–NO and disappearance of Pd^0–CO suggest that both Pd^0–NO and Pd^0–CO compete for the same Pd^0 site.

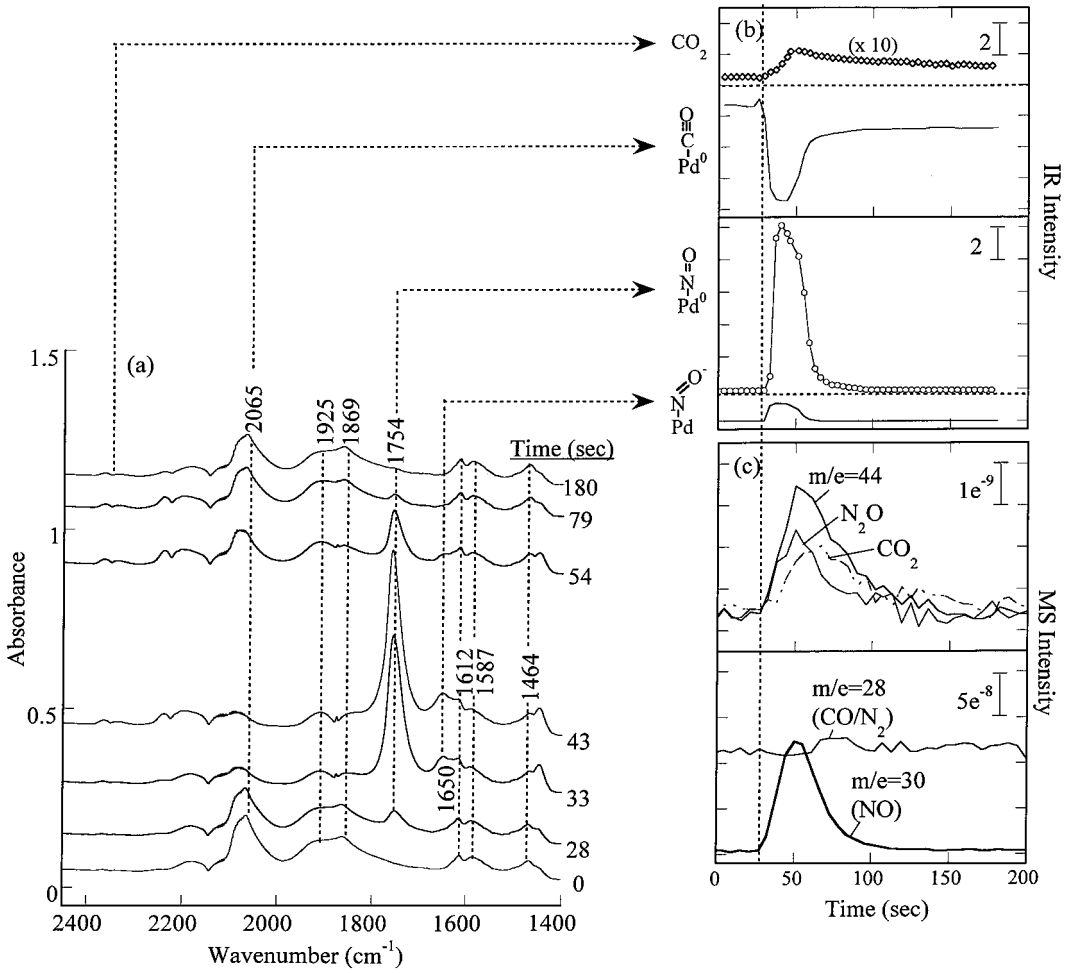

FIG. 5. (a) Transient IR spectra during the NO pulse (10 cm^3) into CO/He (10/30 cm^3/min) flow at 473 K. (b) Integrated area of IR intensity as a function of time. (c) MS intensity profile of the effluent from the IR reactor cell.

One interesting feature of the results in Figs. 7c and 7d is that the CO_2 formation profile leads the IR profile of Pd^0–CO and MS profile of CO/N_2. The results indicate that adsorbed oxygen, produced from the prolonged exposure of the catalyst to NO, is readily available for the reaction with adsorbed CO during the CO pulse. After gaseous CO left the reactor, Pd–NO^+ and Pd–NO^- increased in their intensities along with a small amount of Pd–NCO, which remained on the surface.

Figures 8a–8c show the IR spectra, variation in the IR intensity of adsorbates, and the MS intensity of the effluent from the IR reactor cell during the CO pulse into the NO/He flow at 623 K. Exposure of the catalyst to the NO/He flow produced Pd–NO^+ at 1796 cm^{-1} and nitrate at 1574 cm^{-1}. Al–NCO at 2241 cm^{-1} was produced during the CO pulse at lower temperatures. Pulsing CO caused: (i) a decrease in the intensity of Pd–NO^+, (ii) an increase in the intensity of Al–NCO and carbonate in the 1400–1631 cm^{-1} range, and (iii) an increase in the MS response of CO_2. Due to the high rate of adsorption, desorption, and surface reaction processes, the lead–lag relationship for adsorbates and gaseous species at 623 K is not as obvious as for those at 473 K.

The pulse reaction studies have also been carried out at 523 and 573 K. The 523 K is below light-off where the dynamic behaviors of gaseous and adsorbed species are similar to those at 473 K; and the 573 K is above light-off where the dynamic behaviors of gaseous and adsorbed species are similar to those at 623 K (21).

DISCUSSION

Variation of adsorbate intensity (i.e., relative concentration) with temperature and reactant partial pressure reflects the dependence of the adsorbate formation rate and adsorbate disappearance rate (i.e., adsorbate reactivity) on reaction conditions (9, 11, 22–25). The steps involved in adsorbate formation and disappearance during the NO–CO reaction on Pd/Al_2O_3 are listed in the proposed mechanism in Table 2, which shows the steps that account for the observation of various adsorbates below and above the light-off

TABLE 2

Proposed Mechanism for the NO–CO Reaction

Adsorption and desorption		
Step 1	$Pd^0 + NO \rightleftarrows Pd^0{-}N{=}O$	(linear NO)
Step 2	$Pd^0 + CO \rightleftarrows Pd^0{-}C{\equiv}O$	(linear CO)
Step 3	$Pd^0 + NO \rightleftarrows Pd{-}N^{\overset{O^-}{=}}$	(bent NO)
Step 4	$2Pd^0 + CO \rightleftarrows \begin{matrix}Pd^0\\ Pd^0\end{matrix}{>}C{=}O$	(bridged CO)
Step 5	$\begin{matrix}Pd^0\\ Pd^0\end{matrix}{>}C{=}O \xrightarrow{Pd{-}N{=}O} Pd^0{-}C{\equiv}O + Pd^0$	
Surface reaction		
Step 6	$Pd^0{-}N{=}O + Pd^0 \rightleftarrows Pd^0{-}N + Pd{-}O$	
Step 7	$Pd^0 + Pd{-}O \rightleftarrows (Pd^+)_2O^{2-}$	
Step 8	$Pd^+ + NO \rightleftarrows Pd{-}N{\equiv}O^+$	(cationic NO)
Step 9	$Pd^0{-}N + Pd^0{-}N \rightleftarrows 2Pd^0 + N_2$	
Step 10	$Pd^0{-}N{=}O + Pd^0{-}N \rightleftarrows 2Pd^0 + N_2O$	
Step 11	$Pd^0{-}C{\equiv}O + Pd{-}O \rightleftarrows 2Pd^0 + CO_2$	

temperature. All the steps are listed as reversible steps to follow the microscopic reversibility of catalysis. In reality, certain steps may have a significantly faster forward rate than backward rate and vice versa. The proposed mechanism in Table 2 includes the identify of various NO and CO adsorbates, which are usually represented in the literature by a general form (i.e., NO_{ad} and CO_{ad}).

At 473 K, Figs. 3 and 5 show that NO is adsorbed as linear NO [Pd^0–NO] and CO is adsorbed as linear CO [Pd^0–CO], listed as step 1 and 2, respectively, in Table 2. As NO concentration increased in the NO/CO or NO pulses, NO also adsorbed as bent NO [Pd–NO^-] (step 3). Step 4 for the formation of bridged CO [$(Pd^0)_2$–CO] occurred during the pure CO flow as shown in Fig. 5a. $(Pd^0)_2$–CO was completely removed as NO adsorbed on the Pd surface during the NO pulse into the CO/He flow. Coadsorption of NO and CO studies on Pd[110] has shown that Pd^0–NO destabilizes $(Pd^0)_2$–CO and stabilizes Pd^0–CO, promoting conversion of $(Pd^0)_2$–CO to Pd^0–CO as shown in step 5 (8). The absence of a strong $(Pd^0)_2$–CO band in the NO–CO TPR and the NO/CO pulse studies agrees with these observations.

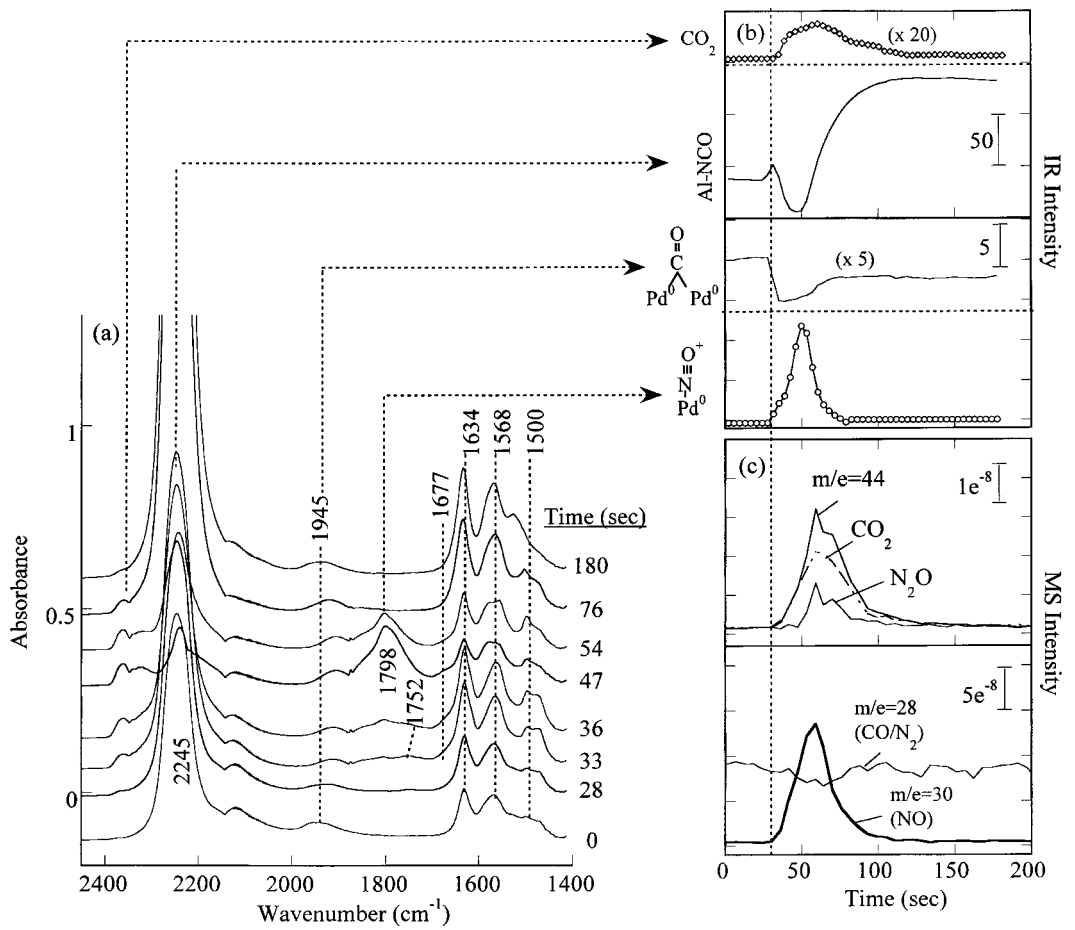

FIG. 6. (a) Transient IR spectra during the NO pulse (10 cm^3) into CO/He (10/30 cm^3/min) flow at 623 K. (b) Integrated area of IR intensity as a function of time. (c) MS intensity profile of the effluent from the IR reactor cell.

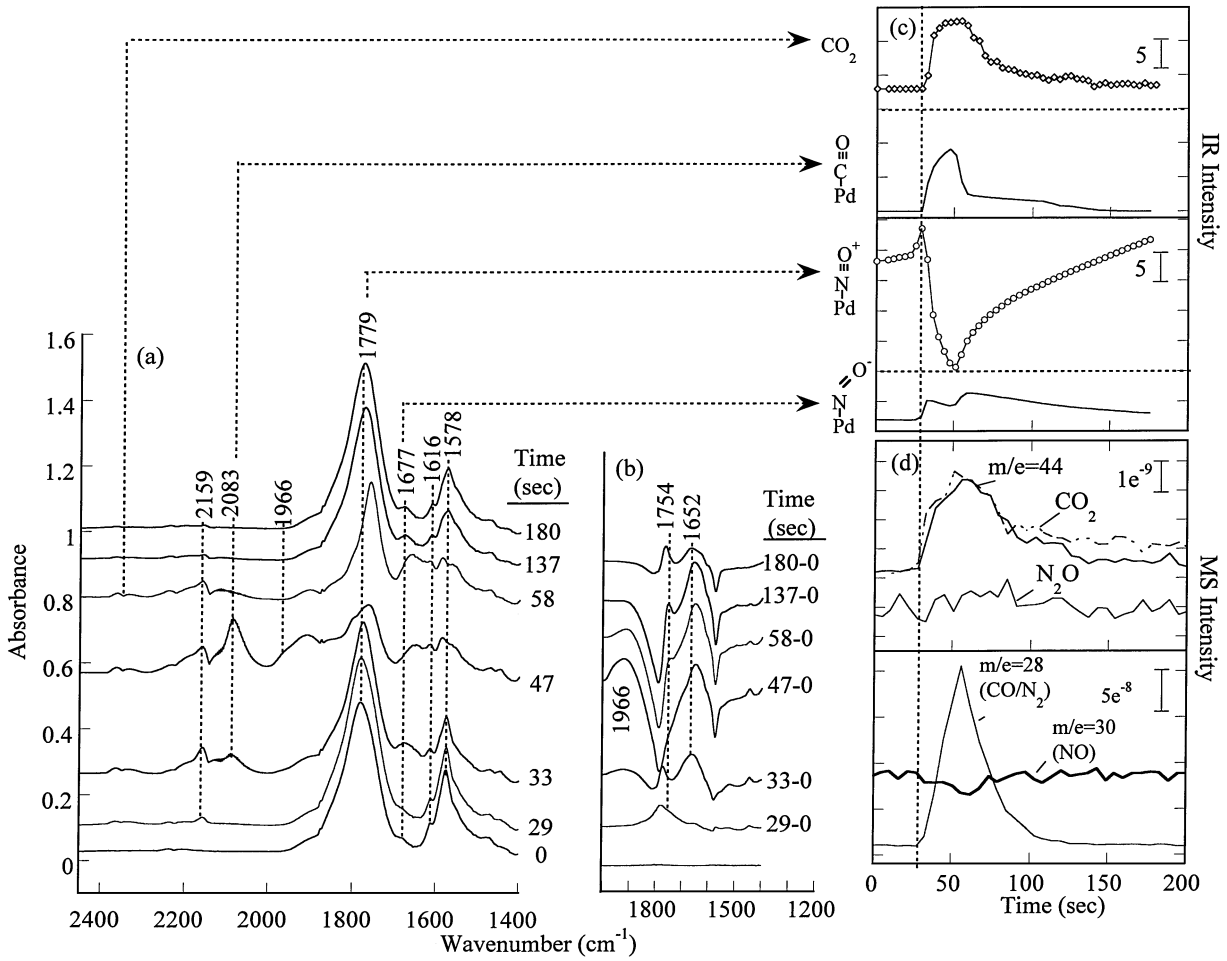

FIG. 7. (a) Transient IR spectra during the CO pulse (10 cm^3) into NO/He (10/30 cm^3/min) flow at 473 K. (b) The difference spectra resulted from the subtraction of the first spectrum from the subsequent spectrum (e.g., 29–0 resulted from the difference between spectra at 29 and 0 s; spectrum at 180–0 resulted from the difference between spectra at 180 and 0 s. (c) Integrated area of IR intensity as a function of time. (d) MS intensity profile of the effluent from the IR cell reactor.

The key steps for the NO–CO reaction are the dissociation of adsorbed NO (step 6) and the removal of adsorbed oxygen from the catalyst surface by reaction with adsorbed CO to form CO_2 (step 11). Adsorption and reaction studies on Pd and Rh single crystal surfaces have suggested that the dissociation of adsorbed NO requires vacant sites (26, 27). However, no clear identity of the form of adsorbed NO involved in NO dissociation has been experimentally determined. It has been suggested that M–NO^- (M = metal atom) is easier to dissociate than M–NO, due to the tilted transition state and electron donation from M to NO (28, 29). Furthermore, the low N–O stretching frequency has been suggested as an indication of the weakening of the N–O bond (23). As a result, the low wavenumber of adsorbed NO (i.e., M–NO^-) should have a higher tendency to dissociate than the high wavenumber of adsorbed NO (i.e., M–NO) (18). However, our recent selective enhancement/poisoning studies have revealed that Pd^0–NO is an active precursor for NO dissociation in the NO–CO reaction (11). The dissociation of this species (step 6) could trigger a series of surface reactions listed in Table 2 for the formation of N_2O, N_2, and CO_2.

The dynamic behavior of Pd^0–NO can be examined by the variation of its IR intensity under the various reaction conditions of the present work. During the NO/CO pulse shown in Fig. 3a, Pd^0–NO increased in intensity with a small variation in its wavenumber followed by a slow decrease in its intensity to one-third of its maximum. Figure 3a also shows that CO_2 formation (step 11) occurs while the wavenumber of Pd^0–NO remains unchanged. The little variation in Pd^0–NO wavenumber with its intensity was also observed during the NO pulse into CO flow as shown in Fig. 5a. These behaviors reflect the absence of dipole–dipole coupling between the neighboring adsorbates of the same type of Pd^0–NO. The Pd^0–NO could be surrounded by adsorbed CO or other adsorbates which are IR-inactive. Therefore, it can be concluded that Pd^0–NO and Pd–NO^-, which followed the same behavior as Pd^0–NO, form a mixed domain (30) with

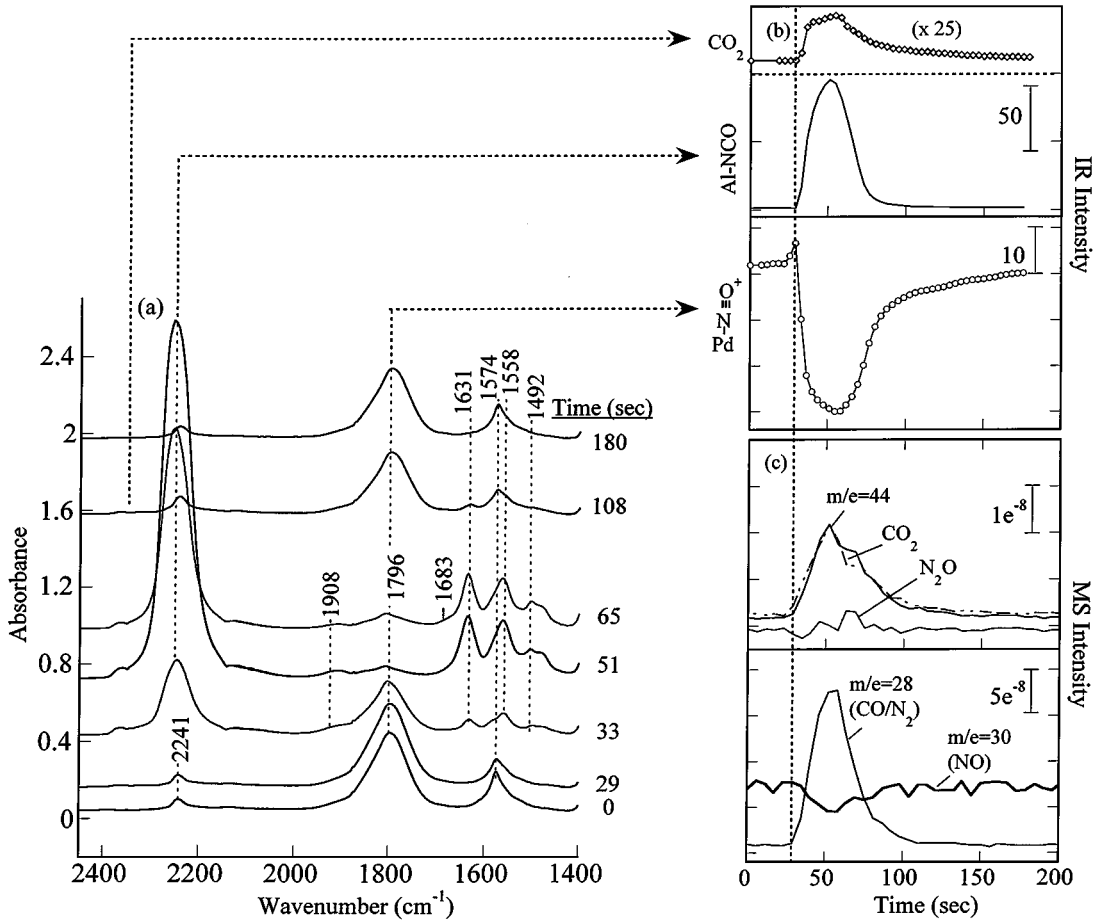

FIG. 8. (a) Transient IR spectra during the CO pulse (10 cm^3) into NO/He (10/30 cm^3/min) flow at 623 K. (b) Integrated area of IR intensity as a function of time. (c) MS intensity profile of the effluent from the IR reactor cell.

CO during the pulse reaction. A mixed domain of NO and CO was also observed on Pd[100] and Pd[111] (9).

Step 9, N_2 formation (31–34), is a facile reaction which has been observed for NO temperature programmed desorption (TPD) on various metal and metal oxide catalysts (35–37). The N_2 formation can be used as a measure to determine whether NO dissociation has occurred on a specific catalytic material or not. The temperature at which NO dissociation started depended on the surface structure and surface coverage of NO adsorbate (29, 38). The general observation is that adsorbed NO can dissociate to adsorbed nitrogen and adsorbed oxygen, leading to the formation of various N-containing products such as N_2, N_2O, and NO_2. N_2O is favorable at low temperatures, whereas N_2 is selectively formed at a higher temperature (31). Step 10 suggests the N_2O formation on Pd^0 sites. This step is supported by the immediate formation of N_2O when NO is pulsed into CO over reduced Pd (Fig. 5a) and by N_2O formation following the disappearance of Pd–NO^+ (Fig. 6a).

Due to overlapping of IR spectra of adsorbed oxygen with that of Al_2O_3, the behavior of adsorbed oxygen could not be observed from IR study; its behavior must be inferred from the IR spectra of adsorbed CO, adsorbed NO, and CO_2. Since $(Pd^0)_2$–CO was absent in the presence of NO, Pd^0–CO would be the most likely CO adsorbate involved in the reaction with adsorbed oxygen (step 11). Figures 3b and 3c show that the Pd^0–CO profile slightly led that of CO_2 during the NO/CO pulse into the He flow; Figs. 5b and 5c show that the Pd^0–CO profile evolved in an opposite direction to that of CO_2 during the NO pulse into the CO flow; Figs. 7c and 7d show that the CO_2 profile slightly led that of Pd^0–CO during the CO pulse into the NO flow. All these observations at 473 K can be explained by the high availability of adsorbed oxygen for the reaction with Pd^0–CO to produce CO_2. The readily available adsorbed oxygen suggests that the dissociation of adsorbed NO is a facile step while the reaction of adsorbed oxygen with Pd^0–CO (step 11) may be the rate-limiting step for the NO–CO reaction, as suggested by other studies (31, 39). Although the breaking of the N–O bond is highly endothermic, involvement of the N–O bond breaking with the catalyst in step 6 (where the products are adsorbed nitrogen

and adsorbed oxygen) changed the endothermicity of the step. The suggested facile nature of the dissociation of adsorbed NO is consistent with the prevailing observations of NO dissociation on various metal and metal oxide catalysts during NO TPD (35–37).

Adsorbed oxygen not only reacted with Pd^0–CO but also played a critical role in affecting the oxidation state of Pd surface atoms. Adsorbed oxygen, produced from prolonged exposure of the reduced Pd to gaseous NO, oxidized Pd^0 to Pd^+ (step 7). It should be noted that this step is written to indicate that adsorbed oxygen may oxidize Pd^0 to Pd^+. The actual stoichiometry of the step is unclear. Formation of Pd^+ is best demonstrated by the appearance of Pd–NO^+ (step 8) as shown in Fig. 7a. CO can reduce Pd^+ to Pd^0, which in turn chemisorbed CO as Pd^0–CO. Results in Fig. 7a suggest that the sequence of the reduction process involved may be:

$$(Pd_2^+)O^{2-} + CO \leftrightarrows 2Pd^0 + CO_2 \quad [1]$$

$$Pd^0 + CO \leftrightarrows Pd^0\text{–}C{\equiv}O. \quad [2]$$

It should be noted that the above two steps are the overall reactions consisting of a set of elementary steps. The occurrence of [1] prior to [2] is supported by the Pd–CO profile, which lagged behind that of CO_2 as shown in Fig. 7c.

Prolonged exposure of the Pd surface to gaseous NO at 473 K is required for producing Pd^+ needed for the formation of Pd–NO^+; and exposure of the Pd surface to gaseous CO caused rapid reduction of Pd^+ to Pd^0 for chemisorption of CO as Pd^0–CO and NO as Pd^0–NO(Fig. 7a). In contrast, at 623 K a short exposure of Pd to the NO/CO pulse into He flow and the NO pulse into CO/He produced Pd^+ for Pd–NO^+ adsorption as shown in Figs. 4a and 6a; exposure to CO caused a decrease in the Pd–NO^+ intensity, reflecting reduction of Pd^+ to Pd^0. However, neither Pd^0–CO nor Pd^0–NO was observed at 623 K. The difference in concentration and behavior of adsorbed CO and NO on the Pd surface at 473 and 623 K suggests a strong dependence of the rates of oxidation (step 7) and reduction (step 11) on temperature. The absence of Pd^0–CO or Pd^0–NO at high temperatures indicates that their desorption and reaction rates are greater than their rate of formation (i.e., adsorption). Absence of Pd–NO^+ at 473 K and its appearance at 623 K under pulse reaction conditions suggests that the rate of the oxidation process of Pd^0 to Pd^+ increased more rapidly with temperature than that of the reduction process.

Prolonged exposure of Pd/Al_2O_3 catalyst to gaseous NO not only oxidized Pd^0 to Pd^+, but also produced nitrate species on the Al_2O_3 surface while exposure of the catalyst to gaseous CO reduced Pd^+ to Pd^0 and produced carbonate on the Al_2O_3 surface, regardless of the initial state of the catalyst surface. Pulse reaction studies on the catalyst, prereduced in flowing H_2 at 673 K between each pulse study, further confirms that the initial catalyst state and adsorbed species on the Al_2O_3 surface did not alter the dynamic behavior of adsorbed species on the Pd surface under reaction conditions and that no memory effect was observed (21). The states of Pd surface established by preadsorption of H_2, O_2, NO, or CO are rapidly modified to the state containing Pd^0 or/and Pd^+, depending on reaction conditions. This is in contrast to the observation of significant memory effect on Rh/Al_2O_3 catalyst on which prereduction and preoxidation significantly changed the forms of adsorbed NO and CO as well as the steady-state and pulse reaction rates (40). Lack of memory effect could be the reason why Pd catalysts are more durable than Rh/Pt catalysts.

In comparison with Rh catalysts, the Pd^0 atoms are more resistant to oxidation than Rh^0atoms below light-off. The oxidation of Rh^0 to Rh^+ has been observed under very mild reaction conditions (e.g., NO/CO = 1/100 and $T = 300$ K), which produces gem-dicarbonyl [Rh^+–$(CO)_2$] (41). On a per site basis comparison, the Pd/Al_2O_3 is more active than 5 wt% Rh/SiO_2, as shown in Table 1. High activity of Pd may be associated with its resistance to oxidation and ability to maintain the Pd^0 reduced state.

High IR intensity of Al–NCO was observed above light-off. It has been demonstrated that the Al–NCO species is formed by the following steps (where M^0 is the reduced site and includes Rh, Pd, Ru, and Pt) (11, 15–18):

$$M^0\text{–N} + M^0\text{–CO} \rightarrow M^0\text{–NCO} + M^0$$

$$M^0\text{–NCO} + \text{Al} \rightarrow M^0 + \text{Al–NCO}.$$

The surface coverage of M^0–NCO increased with CO partial pressure and decomposed when the reduction of NO stopped on Rh/SiO_2 at 500 K (17). The present study shows that the Al–NCO intensity exhibits an initial increase and then gradually decays during the NO/CO pulse (Fig. 4a), levels off after the NO pulse into CO (Fig. 6a), and rapidly decays after the CO pulse into NO (Fig. 8a). These observations suggest that reducing environment is needed for the stability of the Al–NCO species. Such a requirement is also evident by the decrease in the Al–NCO intensity accompanied with an increase in the Pd–NO^+ intensity in an oxidizing environment produced by pulsing NO (Fig. 6a).

CONCLUSIONS

In situ IR coupled with TPR and pulse reaction studies allows observation of various forms of adsorbed NO and CO species under a wide range of reaction conditions. Below the light-off temperature (i.e., 561 K), Pd^0–NO and Pd^0–CO are dominant NO and CO adsorbates. Pd^0–NO competes favorably over Pd^0–CO for the same Pd^0 site when the temperature is increased. Pulse reaction studies at 473 K suggest that Pd^0–NO dissociates to form adsorbed nitrogen and adsorbed oxygen. Adsorbed oxygen further reacts

with Pd^0–CO to produce CO_2. Dynamic behavior of adsorbed NO and CO as well as gaseous products suggests that removal of adsorbed oxygen from the Pd surface to produce CO_2 is the rate-limiting step. Prolonged exposure of the catalyst to the NO flow at 473 K results in oxidation of Pd^0 to Pd^+ and produces Pd–NO^+; the presence of gaseous CO reduces Pd^+ to Pd^0 and increases the surface coverage of Pd^0–NO. Above the light-off temperature, Pd–NO^+, Al–NCO, nitrate, and carbonate are the dominant adsorbates. The presence of Pd–NO^+ indicates that the process of oxidation of Pd^0 to Pd^+ by NO is faster than that of the reduction of Pd^+ to Pd^0 by CO. All the gaseous reaction products are produced on Pd^0 sites.

ACKNOWLEDGMENT

This work was supported by the National Science Foundation under Grant CTS-942111996.

REFERENCES

1. Shelef, M., *Catal. Rev. Sci. Eng.* **11**, 1 (1975).
2. Oh, S. H., Fisher, G. B., Carpenter, J. E., and Goodman, D. W., *J. Catal.* **100**, 360 (1986).
3. Schwartz, S. B., Fisher, G. B., and Schmidt, L. D., *J. Phys. Chem*. **92**, 389 (1988).
4. Summers, J. C., and Williamson, W. B., *in* "Environmental Catalysis" (J. N. Armor, Ed.), ACS Symposium Series, Vol. 552, p. 96. American Chemical Society, Washington, DC, 1994.
5. Monroe, D. R., Krueger, M. H., Beck, D. D., and D'Aniello, M. J., Jr., *in* "Catalysis and Automotive Pollution Control II" (A. Crucq, Ed.), Vol. 71, p. 667. Elsevier Science, Amsterdam, 1991.
6. Beck, D. D., Sommers, J. W., and DiMaggio, C. L., *Appl. Catal. B* **3**, 205 (1994).
7. Grill, C. M., and Gonzalez, R. D., *J. Phys. Chem*. **84**, 878 (1980).
8. Raval, R., Blyholder, G., Haq, S., and King, D. A., *J. Phys. Condens. Matter* **1**, SB165, (1989).
9. Xu, X., Chen. P., and Goodman, D. W., *J. Phys. Chem*. **98**, 9242 (1994).
10. Hoost, T. E., Otto, K., and Laframboise, K. A., *J. Catal*. **155**, 303 (1995).
11. Almusaiteer, K., and Chuang, S. S. C., *J. Catal*. **180**, 161 (1998).
12. Valden, M., Keiski, R. L., Xiang, N., Pere, J., Aaltonen, J., Pessa, M., Maunula, T., Savimaki, A., Lahti, A., and Harkonen, M., *J. Catal*. **161**, 614 (1996).
13. Bell, A. T., and Hegedus, L. L. (Eds.), *in* "Catalysis Under Transient Conditions," ACS Symposium Series 178. American Chemical Society, Washington, DC, 1982.
14. Chuang, S. S. C., Brundage, M. A., Balakos, M. W., and Srinivas, G., *Appl. Spectrosc.* **49**, 1151 (1995).
15. Unland, M. L., *J. Catal.* **31**, 459 (1973).
16. Solymosi, F., and Rasko, J., *J. Catal.* **63**, 217 (1980).
17. Hecker, W. C., and Bell, A. T., *J. Catal.* **85**, 389 (1984).
18. Krishnamurthy, R., and Chuang, S. S. C., *J. Phys. Chem*. **99**, 16727 (1995).
19. Nakamoto, K., "Infrared and Raman Spectra of Inorganic and Coordination Compounds." Wiley, New York, 1986.
20. Krishnamurthy, R., and Chuang, S. S. C., and Balakos, M. W., *J. Catal.* **157**, 512 (1995).
21. Almusaiteer, K., Ph.D. dissertation, The University of Akron, Akron, OH, 1999.
22. Yates, J. T., Jr., Duncan, T. M., Worley, S. D., and Vaughan, R. W., *J. Phys. Chem*. **70**, 1219 (1979).
23. Hecker, W. C., and Bell, A. T., *J. Catal.* **84**, 200 (1983).
24. Dictor, R., *J. Catal.* **109**, 89 (1988).
25. Chuang, S. S. C., and Tan, C.-D., *J. Catal.* **173**, 95 (1998).
26. Masel, R. I., "Principles of Adsorption and Reaction on Solid Surfaces," p. 757. Wiley, New York, 1996.
27. Root, T. W., Fisher, G. B., Schmidt, L. D., *J. Chem. Phys.* **85**, 4679 (1986).
28. Connelly, N. G., *Inorg. Chim. Acta* **6**, 47 (1972).
29. Villarubia, J. S., and Ho, H., *J. Chem. Phys.* **87**, 750 (1987).
30. Gates, B. C., "Catalytic Chemistry," p. 356. Wiley, New York, 1992.
31. Cho, B. K., Shanks, B. H., and Bailey, J. E., *J. Catal.* **115**, 486 (1989).
32. Oh, S. H., *J. Catal.* **124**, 477 (1990).
33. Taylor, K. C., *Catal. Rev. Sci. Eng.* **35**, 457 (1993).
34. Ng, K. Y. S., Belton, D. N., Schmeig, S. J., and Fisher, G. B., *J. Catal.* **146**, 394 (1994).
35. Sugai, S., Watanabe, H., Kioka, T., Miki, H., and Kawasaki, K., *Surf. Sci.* **259**, 109 (1991).
36. Ramsier, R. D., Gao, Q., Waltenburg, H. N., Lee, K. W., Nooij, O. W., Lefferts, L., and Yates, J. T., Jr., *Surf. Sci.* **320**, 209 (1994).
37. Cordatos, H., and Gort, R. J., *Appl. Catal. B* **7**, 33 (1995).
38. Wolf, R. M., Bakker, J. W., and Nieuwenhuys, B. E., *Surf. Sci.* **246**, 135 (1991).
39. Rainer, D. R., Koranne, M., Vesecky, S. M., and Goodman, D. W., *J. Phys. Chem*. **101**, 10769 (1997).
40. Almusaiteer, K., and Chuang, S. S. C., in preparation.
41. Solymosi, F., Bansagi, T., and Novak, E., *J. Catal.* **112**, 183 (1988).